Bioorganic Chemistry 113 (2021) 104982

Contents lists available at ScienceDirect

Bioorganic Chemistry

journal homepage: www.elsevier.com/locate/bioorg

Synthesis, biological evaluation and molecular docking studies of novel 1,2,3-triazole-quinazolines as antiproliferative agents displaying ERK inhibitory activity

Paulo Sérgio Gonçalves Nunes [a], Gabriel da Silva [b], Sofia Nascimento [c], Susimaire Pedersoli Mantoani [a], Peterson de Andrade [a], Emerson Soares Bernardes [c], Daniel Fábio Kawano [d], Andreia Machado Leopoldino [b], Ivone Carvalho [a,*]

[a] School of Pharmaceutical Sciences of Ribeirão Preto, University of São Paulo, Ribeirão Preto, São Paulo, Brazil
[b] Department of Clinical Analyses, Toxicology and Food Sciences, School of Pharmaceutical Sciences of Ribeirão Preto, University of São Paulo, Ribeirão Preto, São Paulo, Brazil
[c] Radiopharmacy Center, Nuclear and Energy Research Institute (IPEN/CNEN-SP), São Paulo, São Paulo, Brazil
[d] Faculdade de Ciências Farmacêuticas, Universidade Estadual de Campinas, Campinas, São Paulo, Brazil

ARTICLE INFO

Keywords:
4-aminoquinazolines
Click Chemistry
ERK kinase

ABSTRACT

ERK1/2 inhibitors have attracted special attention concerning the ability of circumventing cases of innate or long-term acquired resistance to RAF and MEK kinase inhibitors. Based on the 4-aminoquinazoline pharmacophore of kinases, herein we describe the synthesis of 4-aminoquinazoline derivatives bearing a 1,2,3-triazole stable core to bridge different aromatic and heterocyclic rings using copper-catalysed azide-alkyne cycloaddition reaction (CuAAC) as a Click Chemistry strategy. The initial screening of twelve derivatives in tumoral cells (CAL-27, HN13, HGC-27, and BT-20) revealed that the most active in BT-20 cells (**25a,** IC_{50} 24.6 μM and a SI of 3.25) contains a more polar side chain (sulfone). Furthermore, compound **25a** promoted a significant release of lactate dehydrogenase (LDH), suggesting the induction of cell death by necrosis. In addition, this compound induced G0/G1 stalling in BT-20 cells, which was accompanied by a decrease in the S phase. Western blot analysis of the levels of p-STAT3, p-ERK, PARP, p53 and cleaved caspase-3 revealed p-ERK1/2 and p-STA3 were drastically decreased in BT-20 cells under **25a** incubation, suggesting the involvement of these two kinases in the mechanisms underlying **25a**-induced cell cycle arrest, besides loss of proliferation and viability of the breast cancer cell. Molecular docking simulations using the ERK-ulixertinib crystallographic complex showed compound **25a** could potentially compete with ATP for binding to ERK in a slightly higher affinity than the reference ERK1/2 inhibitor. Further *in silico* analyses showed comparable toxicity and pharmacokinetic profiles for compound **25a** in relation to ulixertinib.

1. Introduction

Malignant tumors encompassing uncontrolled cell growth and metastasis is an alarming and devastating disease that affects about 18 million people annually (2019) and accounts for 9.6 million deaths (2018), placing the disease as the second leading cause of death globally, mainly in low- and middle-income countries (70%) [1,2]. Even in this scenario, advances in cancer chemotherapy had a significant contribution to patient survival rates since, in association with an increase in screening campaigns, they will reduce the development of advanced stage tumours [3]. In fact, effective combination therapy has evolved dramatically, although many of these drugs act against common targets found in normal and cancer cells. Cytotoxic drugs, for instance, can induce selective DNA damage based on its higher concentration in cancer cells that replicate and grow faster than normal cells. However, a range of limitations have arisen as these conventional cytotoxic drugs may not reach a dormant tumour besides inducing harmful side effects to patients due to the lack of selectivity towards rapid grow normal cells. To address these issues, a better understanding of genetic and molecular biology of cancer cells has emerged and led to the molecular target

* Corresponding author.
E-mail address: carronal@usp.br (I. Carvalho).

https://doi.org/10.1016/j.bioorg.2021.104982
Received 6 January 2021; Received in revised form 23 April 2021; Accepted 5 May 2021
Available online 11 May 2021

therapeutic discovery of highly selective drugs to target a unique or overexpressed protein in cancer cells, with less toxic side effects [4].

Inhibitors of the signalling transduction pathways to target excessive quantities of protein kinases and receptor tyrosine kinases, as well as hamper uncontrolled cell growth and cell division, are already in clinical practise, representing 52 kinases at the end of 2019 [4,5]. Gefitinib (certain breast, lung cancers) and imatinib (chronic myelogenous leukaemia, CML) are milestones in anticancer therapy that affect the phosphotransfer kinase cascade and target EGFR and hybrid Bcr-Abl tyrosine kinases, respectively. Subsequently, second and third generations of these drugs were introduced to the market to target a range of therapeutically important tyrosine kinases, promote drug selectivity, and circumvent off-target-mediated toxicity and resistance acquired by the original drugs [5,6].

As part of the MAPKs oncogenic cascade that triggers cancer cell proliferation, differentiation, division and prevents apoptosis, the RAS–RAF–MEK–ERK1/2 kinase pathway is unusually activated in more than 30% of human cancers. Although RAS mutations represent most of the MAPK variations (22%) [7], it is usually considered undruggable because of an uncommon affinity for its substrate (GTP) and absence of proper pockets for the development of inhibitors [8]. In this context, the lack of effective RAS inhibitors has pointed to downstream kinases, RAF, MEK and ERK, as potential therapeutic targets. Therefore, selective RAF (vemurafenib and dabrafenib) [9] and MEK inhibitors (trametinib, cobimetinib and binimetinib) are FDA approved drugs used in combination with other kinase (BRAF) inhibitors to reduce the toxicities related to BRAF inhibition and delay the development of drug resistance, though disease recrudescence is usually observed within one year of treatment [10,11].

Therefore, extracellular signal-regulated kinases 1 and 2 (ERK1/2) inhibitors have attracted special attention as they have circumvented cases of innate or long-term acquired resistance to RAF and MEK inhibitors and simultaneously targeted two nodes of the pathway [12]. Several ERK1/2 drug-like small molecules had an IC_{50} in nM range and entered preclinical and phase I clinical trial, such as ulixertinib (K_i ERK2 0.04 nM) [13], which is now being assessed as a single agent (not in association with BRAF inhibitors) for the treatment of several cancers. (Clinicaltrials.gov identifiers: NCT04145297, NCT03698994, NCT04488003, NCT03454035, NCT03155620, NCT02465060). In addition, MK-8353 was discovered as a potent experimental ERK1/2 inhibitor (IC_{50} 20 and 7 nM, respectively) [14], while its close analogue, SCH772984 (IC_{50} 4 nM and 1 nM, respectively) [15], did not provide satisfactory results in patients with advanced solid tumors despite good tolerance [16]. Alternatively, 4-[7-(1-benzyl-1*H*-pyrazol-4-yl)-5*H*-pyrrolo[2,3-*b*]pyrazin-2-yl]pyridine, identified through a fragment-based approach, showed a significant ERK2 inhibition (IC_{50} 37 nM) (Fig. 1A) [17]. Due to structure variations, distinct mechanisms of action were observed and, while the majority acts as reversible inhibitors in an ATP-competitive manner, some are covalent or allosteric ERK1/2 inhibitors [18].

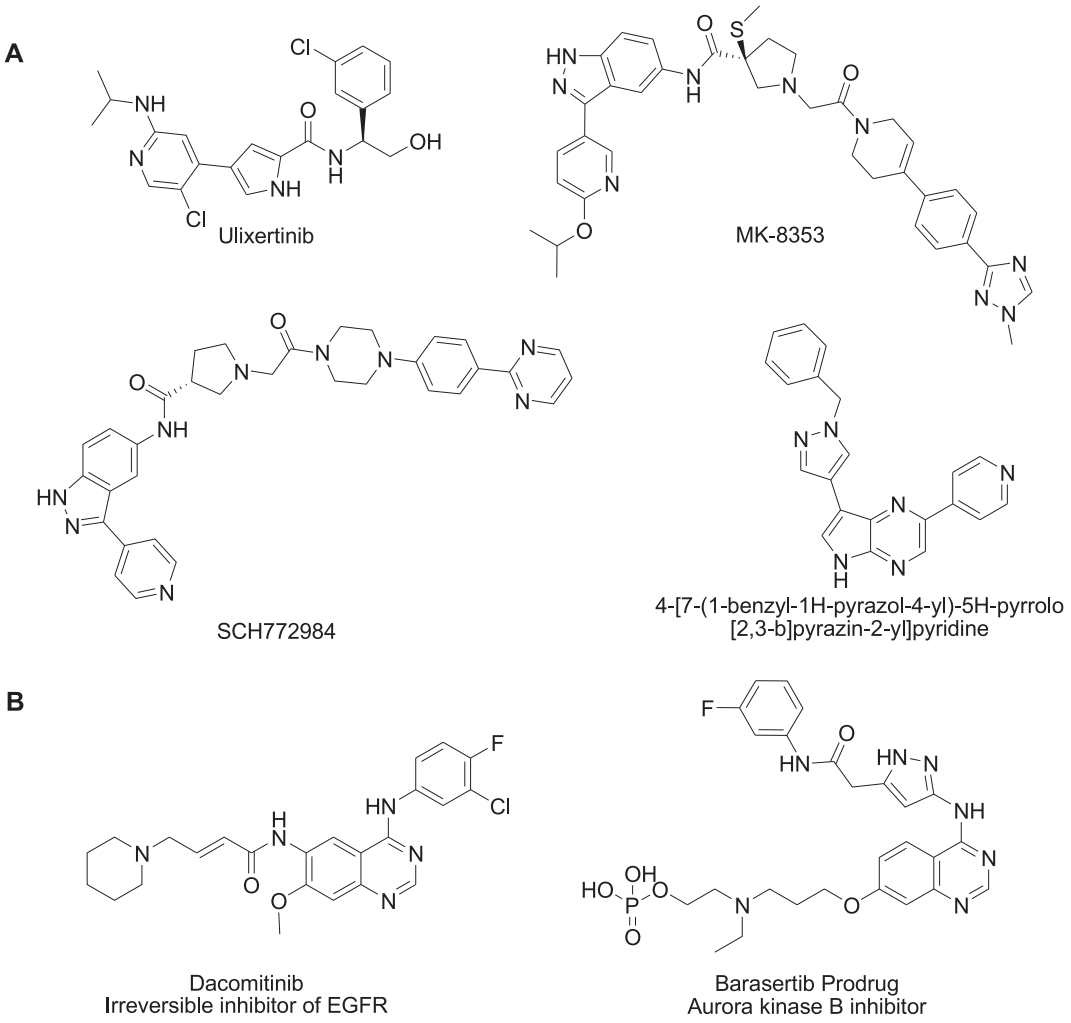

Fig. 1. (A). ERK inhibitors under pre-clinical and clinical trials, ulixertinib, MK-8353, SCH772984 and 4-[7-(1-benzyl-1*H*-pyrazol-4-yl)-5*H*-pyrrolo[2,3-*b*]pyrazin-2-yl] pyridine. **(B)**. The recently approved 4-anilino-quinazoline drug, dacomitinib, and the 4-amino-pyrazoloquinazoline dihydrogen phosphate prodrug, barasertib, under clinical trial.

Amongst kinase inhibitor drugs, it is worth mentioning the fused pyrimidine core related to 4-anilino-quinazoline: gefitinib, erlotinib, afatinib, lapatinib, canertinib, vandetanib and dacomitinib, the latter displaying a K_i value for EGFR of 0.16 ± 0.01 nM [19]. Additionally, the 4-amino-pyrazoloquinazoline dihydrogen phosphate prodrug, barasertib, act as selective Aurora kinase B inhibitor (IC_{50} 0.37 nM) [20], and is under clinical trial (Fig. 1B) [21]. Notably, 4-anilino quinazoline pharmacophore is essential for EGFR tyrosine kinase and HER2/Pan-HER kinase inhibition, while several 4-amino quinazoline derivatives have potential to target checkpoint kinases [22], aurora kinases [23,24], Interleukin-1 receptor associated kinase-4 (IRAK-4) [25,26] and others. Beyond anticancer drugs, quinazolines have broad therapeutic activity and efficacy, such as antimalarial, antimicrobial, antidiabetic, antihypertensive, sedative and anti-inflammatory [27].

As many kinase inhibitors tend to cross-interact with the different enzymes from the class because of the conservation of the catalytic cleft [28], we hypothesized the 5*H*-pyrrolo[2,3-*b*]pyrazin-2-yl] nuclei at the ERK inhibitor 4-[7-(1-benzyl-1*H*-pyrazol-4-yl)-5*H*-pyrrolo[2,3-*b*]pyrazin-2-yl]pyridine could interact similarly as the 4-amino-quinazoline moiety from the Aurora kinase B inhibitor barasertib (Fig. 2). Based on the bioisostere concept, we have also proposed the replacement of the pyrazole groups at these inhibitors by 1,4-disubstituted 1,2,3-triazoles since these groups are known to provide a fast exploration of chemical space through the generation of libraries of analogues [29]. In fact, superposition of the crystallographic structures of both inhibitors (PDB ID 4QPA and 4C2V) showed a good correspondence, as depicted in Fig. S1.

In this context, we designed a small library of eight potential ERK1/2 kinase inhibitors conserving the 4-aminoquinazoline pharmacophore bearing a 1,2,3-triazole stable core to bridge different aromatic and heterocyclic rings using copper-catalysed azide-alkyne cycloaddition reaction (CuAAC) as a Click Chemistry strategy. In addition, four 4-aminoquinazolines previously prepared by our group were also tested [30,31]. The ability of these compounds to affect the cancer cell growth and division was assessed on oral squamous cell carcinoma (CAL-27 and HN13), gastric (HGC-27) and breast (BT-20) cancer cells. The most active compound in BT-20 cells was subjected to further investigations in order to get some insights about its mode of action. Interestingly, this selected compound (**25a**) induced cell death and cell cycle arrest with an increase in the subpopulation of cells in G0/G1 phase, as well as synchronized decrease in the S phase, which was associated with a remarkable decrease of p-ERK1/2 and p-STAT3, as revealed by Western blot analysis. Further molecular modelling studies confirmed the potential interactions of compound **25a** toward ATP site of p-ERK1/2 kinase.

2. Results and discussion

2.1. Synthesis

Initially, the conventional Niementoski cyclocondensation reaction between anthranilic acid derivative **1** (R_1, R_2 = OMe) and formamide under microwave heating was pursued to obtain quinazolin-4(3*H*)-ones **2b** in 70% yields, while the non-substituted **2a** was acquired from commercial source [32]. Although intermediate **2b** was obtained in reasonable yield, the one-pot intermolecular reductive *N*-heterocyclisation of the corresponding methyl 2-nitrobenzoate ester of **3** with formamide was also tested with indium(III) chloride. However, the use of this Lewis acid at high temperature to induce formamide decomposition and form carbon monoxide, for in situ reductive conversion of 2-nitrobenzoate into 2-aminobenzoate derivative, gave the quinazolinone **2b** in low yields (35%) (Scheme 1) [33].

Intermediate **2c**, bearing a benzyloxy group installed at C-6 position of quinazoline core, was obtained through regioselective 5-methoxyl cleavage of 4,5-dimethoxy-2-nitrobenzoic acid (**3**), taking the advantage of the electron withdrawn effect of the *p*-nitro group, which weakens the Ar-OMe bond and makes it more susceptible to nucleophilic attack (OH^-), in a mechanism similar to S_NAr [34]. Under strong basic conditions and at high temperature, the structure of the 5-hydroxy-4-methoxy-2-nitrobenzoic acid intermediate (sole isomer obtained in 91% yield) was ascribed based on the NOE-*diff* experiments, which showed the selective removal of the methyl group at C-5 position based on the presence of NOE only between H-3 and 4-OMe, Fig. S2 [35,36]. This selective cleavage in the early stages of the synthesis proved to be better than the deprotection of the 6,7-dimethoxy-quinazolin-4(3*H*)-one (**2a**) intermediate using methionine, which resulted in an inseparable mixture of both regioisomers on a chromatographic column [37]. After esterification, methyl 5-hydroxy-4-methoxy-nitrobenzoate (**4**) was

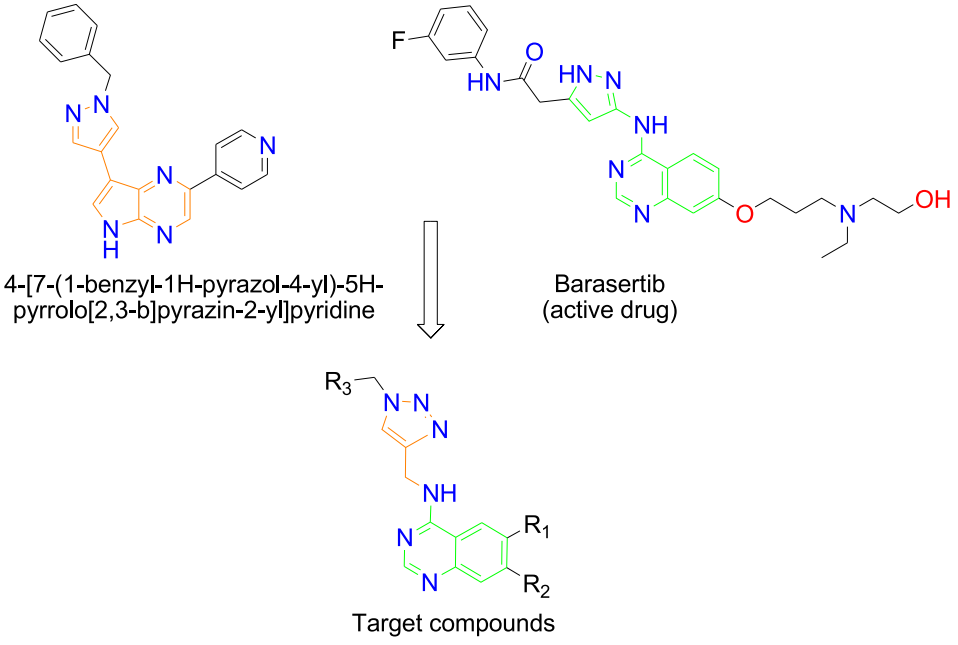

Fig. 2. Design of potential 4-amino-quinazoline-based ERK inhibitors based on the structures of the Aurora kinase B inhibitor barasertib and the ERK2 inhibitor 4-[7-(1-benzyl-1*H*-pyrazol-4-yl)-5*H*-pyrrolo[2,3-*b*]pyrazin-2-yl]pyridine.

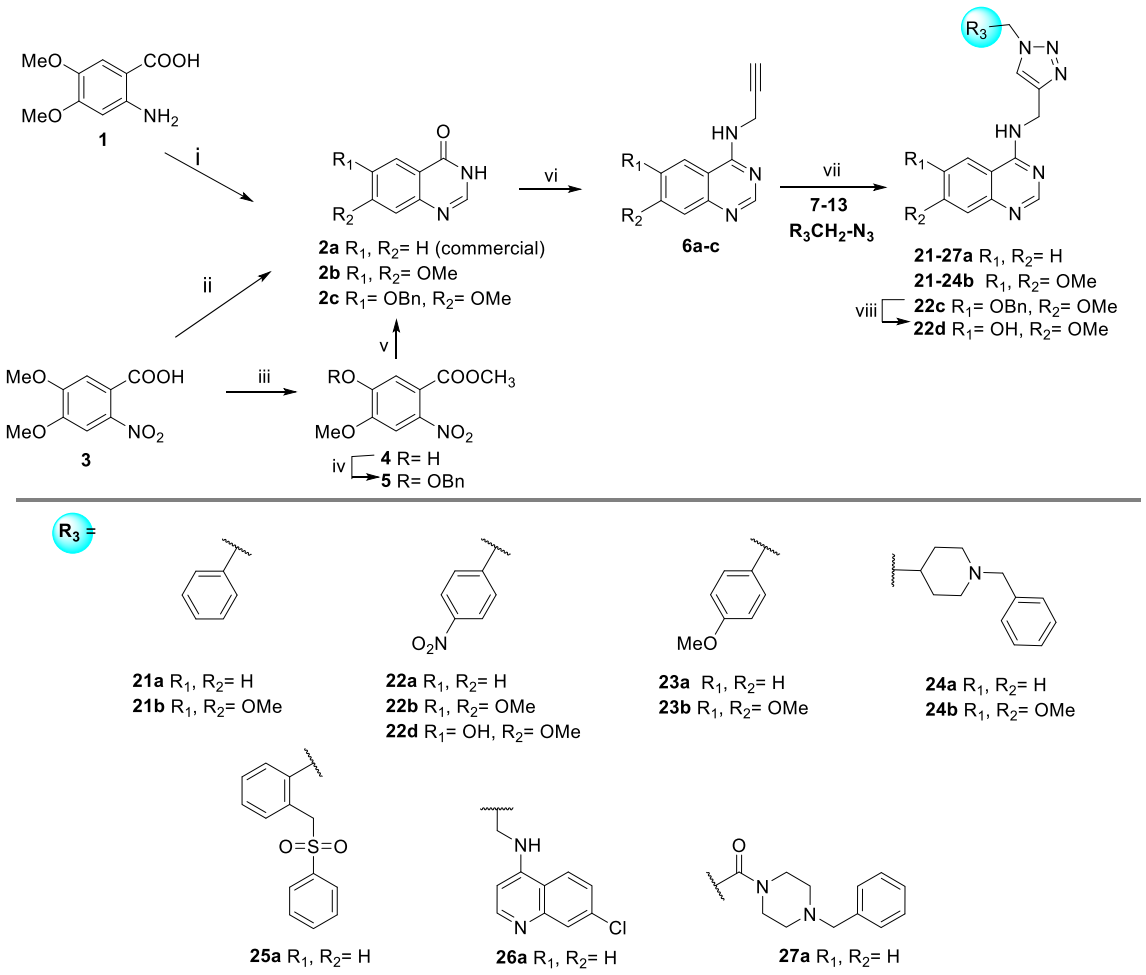

Scheme 1. General procedures for the synthesis of the target compounds **21-24a,b, 25-27a** and **22c,d**. Reagents and conditions: i. formamide, 60 W, 150 °C, 40 min; ii. a) MeOH, H_2SO_4, reflux, 48 h; b) formamide, $InCl_3$, 150 °C; iii. a) NaOH (6 mol.L^{-1}), 100 °C, 3 h, b) MeOH, H_2SO_4, reflux, 48 h; iv. BnBr, Cs_2CO_3, DMF, 24 h; v. formamide, $InCl_3$, 150 °C; vi. PyBOP, DBU, propargylamine, DMF; vii. azide derivatives **7–13** (**R_3CH_2-N_3**), sodium ascorbate, $CuSO_4$, DMF or 1,10-phenantroline, sodium ascorbate, $CuSO_4$, EtOH:H_2O [2:1 (v/v)]; viii. TFA, reflux.

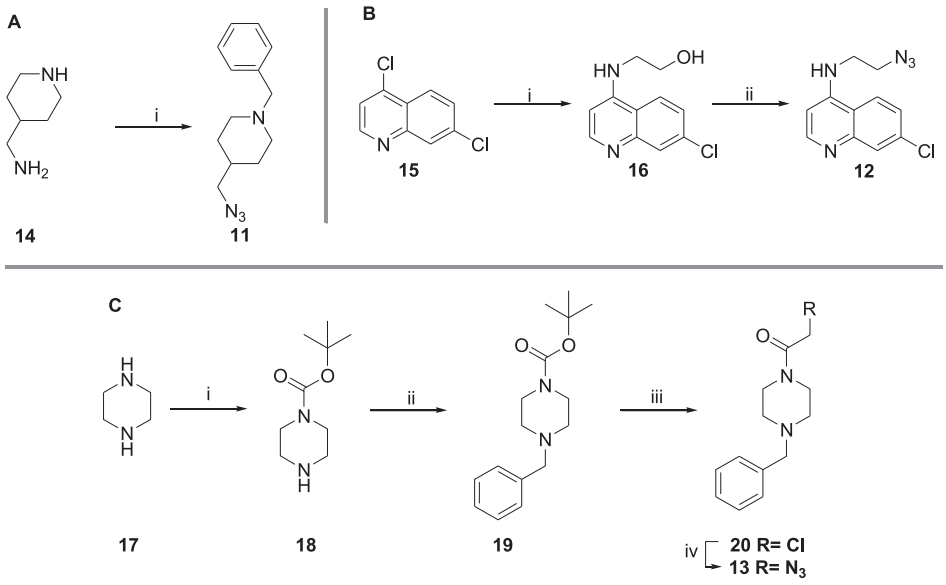

Scheme 2. Synthesis of azides **11**–**13**. Reagents and conditions: **(A).** i. a) 1-(azidosulfonyl)-1*H*-imidazol-3-ium hydrogensulfate, $CuSO_4$, $NaHCO_3$, MeOH, H_2O; b) BnCl, K_2CO_3, acetone. **(B).** i. ethanolamine, triethylamine, 120 °C, 2 h; ii. a) $SOCl_2$, DMF, r.t.; b) NaN_3, DMF. **(C).** i. Boc_2O, DCM, 0 °C, r.t.; ii. BnBr, K_2CO_3, DCM, reflux; iii. a) HCl in dioxane; b) chloroacetyl chloride, DCM, 0 °C, r.t.; iv. NaN_3, DMF, 70 °C, 150 W, 15 min.

readily protected with benzyl bromide to give **5**, which was subjected to one-pot cyclization using the aforementioned formamide and indium chloride to generate the corresponding quinazolinone **2c** (Scheme 1).

Thus, nucleophilic aromatic substitution (S_NAr) was carried out using mild phosphonium-promoted reaction to introduce propargylamine group in quinazolinones (**2a-c**) to give the corresponding *N*-(prop-2-yn-1-yl)quinazolin-4-amine derivatives **6a** (80%), **6b** (55%) and **6c** (57%) [38].

For the cycloaddition reaction with *N*-(prop-2-yn-1-yl)quinazolin-4-amines **6a-c**, azides **7**–**13** (R_3CH_2-N_3) were prepared from the corresponding halide derivatives using sodium azide in DMF. The azides **7**–**10** (SI) were synthesised from commercial halides [39–42], whilst the azides **11**–**13** were obtained according to Scheme 2. Thus, the treatment of 4-(aminomethyl)piperidine (**14**) with 1-(azidosulfonyl)-1*H*-imidazol-3-ium hydrogensulfate azide, followed by benzylation of the secondary amine with BnCl and K_2CO_3 in acetone, afforded azide **11** (Scheme 2A) [30]. On the other hand, addition of ethanolamine at C-4 position of commercial 4,7-dichloroquinoline (**15**) gave intermediate **16**, which was converted to azido **12** under treatment with thionyl chloride, followed by NaN_3 in DMF (Scheme 2B) [43,44]. The route to obtain azide **13** started with mono protection of the commercial piperazine (**17**) with di-*tert*-butyl dicarbonate to produce compound **18** with 78% yield [45,46], followed by treatment with BnBr and K_2CO_3 in DCM under reflux for benzylation of the free secondary amine to obtain compound **19** in reasonable yield (49%) [47]. Removal of the Boc under acidic condition (2.0 mol.L^{-1} HCl in dioxane) and subsequent reaction with chloroacetyl chloride gave compound **20** in excellent yield (86%) [48]. Finally, azide **13** was obtained with 84% yield by S_N2 reaction in the presence of NaN_3 in DMF under microwave irradiation (Scheme 2C).

As for the final step, CuAAC reaction better results were achieved using microwave heating at 100 W, 80 °C for 5 to 10 min with azide precursors **7**–**13** and *N*-(prop-2-yn-1-yl)quinazolin-4-amines **6a-c** (10% excess) in the presence of sodium ascorbate and $CuSO_4$ in DMF [29,42] to give the final products; except compound **22c**, obtained in the presence of 1,10-phenantroline, sodium ascorbate, $CuSO_4$ and EtOH:H_2O [2:1 (v/v) at room temperature]. After purification, the small library of 1,2,3-triazole-quinazoline derivatives **21-24a,b**, **25-27a** and **22c** was obtained as the unique 1,4-disubstituted regioisomer from moderate to good yields (42–72%) and characterized by NMR, which revealed the triazole ^{1}H and the corresponding ^{13}C between 7.55–8.15 ppm (H-12) and 122.9–125.3 ppm (C-12), respectively. The HRMS confirmed the target structures. Compound **22c** was further deprotected to afford **22d** (55%) to be also biologically assessed.

2.2. Biological evaluation

The antitumoral activity of the products **21-24a,b**, **22d** and **25-27a** was evaluated in cancer cell lineages derived from oral squamous cell carcinoma (CAL-27 and HN13), gastric (HGC-27) and breast (BT-20) cancers. The cytotoxicity assay by resazurin was performed at a fixed concentration (50 μM) (Fig. 3).

From the 4-aminoquinazoline series, compounds **21a**, **22a**, **23b**, **24b** and **25a** displayed the most promising antitumoral activities toward BT-20 cells. Thus, the five selected compounds were tested at several concentrations against BT-20 cells and normal fibroblasts (OHMF). The IC_{50} value of compound **25a** at 48 h was 24.6 μM in BT-20 cells and 80 μM in OHMF cells, indicating tumor selectivity over 3-fold (Table 1). In this regard, only compound **25a** displayed a selectivity index (SI) above the minimum threshold (SI ≥ 3) making it a potential compound for further optimization (Table 1). [49].

For the sake of comparison, the reported IC_{50} value for the ERK1/2 inhibitor ulixertinib (please refer to the molecular docking section) against BT-20 cells was 5.7 μM [13]. Considering the interlaboratory variability observed for cell-based cytotoxicity assays [50], we therefore assumed **25a** as a viable structure for further investigation since it performed similarly as this ERK inhibitor, currently under clinical trials.

We then analysed the release of lactate dehydrogenase (LDH) in cell culture media to understand the cytotoxic effect of the compound **25a** in BT-20 cells. The cells exposed to compound **25a** (40 and 80 μM) showed high level of LDH release compared to the negative control (0.01% DMSO), suggesting the induction of cell death by necrosis (Fig. 4A). However, we decided to investigate other mechanisms besides cell death under the action of **25a**, such as cell cycle arrest. The rationale was that the same concentrations used for cytotoxicity and LDH assays did not cause the same intensity of cellular effects.

Given that cell cycle arrest can accompany alterations in the viability assay, we determined the distribution of the BT-20 cells in each cell cycle phase under **25a** exposition. The results in Fig. 4B-C showed that **25a** dose-dependently induced G0/G1 stalling in BT-20 cells. The increase in the subpopulation of cells in G0/G1 was accompanied by a synchronized decrease in the S phase. This has been shown with other ERK inhibitors in melanoma, leukaemia and other human cancers [51–53].

Following findings that **25a** impacts viability and cell cycle progression in BT20 cells, we analysed proteins related to tumour cell signalling by Western blot (Fig. 4D-E). The results indicated the absence of cleaved caspase-3 and PARP protein and reduced p53 levels, suggesting the absence of apoptosis and p53 activation in BT-20 cells incubated

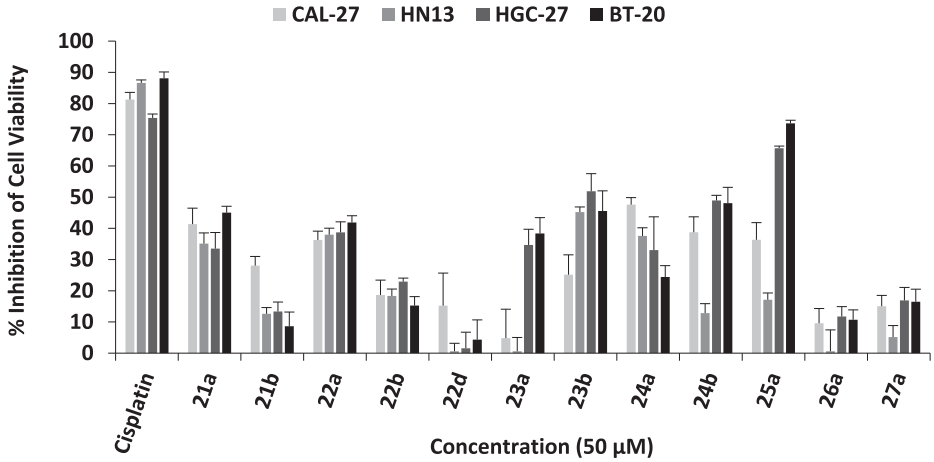

Fig. 3. Inhibition of cell viability by compounds **21-24a,b**, **22d** and **25-27a** was evaluated by the resazurin assay. The cancer cells CAL-27, HN13, HGC-27 and BT-20 were treated with the compounds and cisplatin at 50 μM for 48 h. Two independent biological experiments were performed in quadruplicate. The values are expressed as mean ± standard deviation of % cell viability inhibition.

Table 1
Cytotoxicity profiles of the five selected 4-aminoquinazoline derivatives (**21a**, **22a**, **23b**, **24b** and **25a**) in BT-20 and OHMF cell lineages.

Compound	IC_{50} (μM) (BT-20 cells)	IC_{50} (μM) (OHMF cells)	Selectivity Index (SI)*
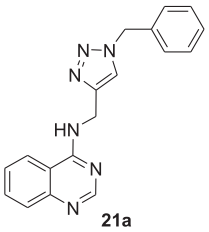 **21a**	>80	>80	–
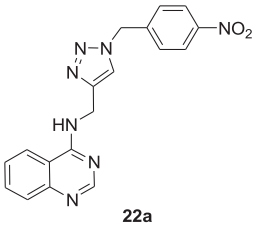 **22a**	>80	>80	–
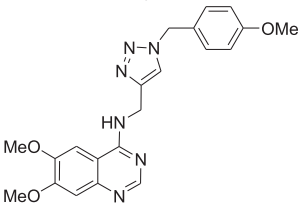 **23b**	>80	>80	–
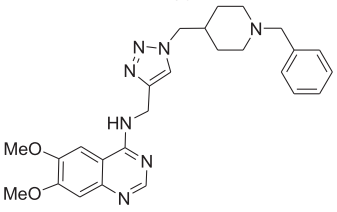 **24b**	24.6 ± 1.06	>80	>3.25
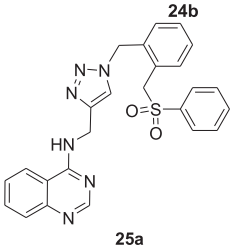 **25a**			

*SI = $IC_{50\_OHMF}/IC_{50\_BT\text{-}20}$. IC = Inhibitory concentration; IC_{50} = concentration that reduces cell viability in 50%. Each experiment was repeated at least three times in quadruplicate, and the percentage of inhibition of cell viability was used to calculate IC_{50} values by nonlinear regression.

with **25a**. On the other hand, our results confirmed that p-ERK1/2 and p-STAT3 were drastically decreased in BT-20 cells under **25a** incubation. Sustained activation of ERK1/2 is essential for G1 to S phase progression, and it can be considered one of the master regulators to cell cycle phase transition [54,55]. Activation of STAT3 is also associated with cell cycle and tumour progression, including in breast cancer cells [56,57]. These results indicated that inactivation of ERK1/2 and STAT3 pathway signalling are mechanisms underlying **25a**-induced cell cycle arrest (20 and 40 μM) accompanied by loss of proliferation and viability in the breast cancer cell.

2.3. Molecular docking

To assess whether **25a** could inhibit the ERK enzyme, we outlined molecular docking simulations with the crystallographic structure of this conserved serine/threonine kinase, which can be activated by phosphorylation on both the threonine/tyrosine residues of a conserved motif (Thr-Glu-Tyr). Triggered by the release of growth factors, its activation is particularly essential for cell cycle progression at the G1 phase, in which persistent and elevated ERK activities allow cells to entry the S phase [58].

As more than one-third of the clinically relevant tumors display constitutively activated ERK enzymes [59], MEK/ERK pathway inhibitors have previously been designed [11]. An important ATP-competitive ERK1/2 inhibitor (ulixertinib - BVD-523) has recently gained attention due to its ability of inducing, alone, tumor regression in xenograft models that are cross-resistant to both BRAF and MEK inhibitors [11]. Based on the ERK inhibition profile suggested for **25a** in the biological assays, we performed molecular docking simulations to compare its most probable binding mode with the corresponding mode predicted for ulixertinib.

The kinase site of serine/threonine kinases lies at the junction of the N- and C-domains, where the adenosine triphosphate (ATP) binds to donate phosphate groups, providing the energy necessary in the reactions catalyzed by these enzymes. Selective kinase inhibitors can be generally categorized as competitive ATP inhibitors, which can bind to the active and/or inactive kinase forms, or allosteric modulators, where the allosteric site can be contiguous or not to the ATP binding cleft [60]. As suggested by the docking simulations, both ulixertinib (Fig. 5A) and **25a** (Fig. 5B) compete with ATP for binding to the ERK with a slightly higher affinity observed for **25a** than for the reference ERK1/2 inhibitor: $\Delta G_{binding} = -6.6$ and -5.6 kcal/mol, respectively.

Interestingly, **25a** seems to interact with the residues from the ATP binding cleft more efficiently than ulixertinib, with an almost perfect superposition between its terminal phenyl ring with the heteroaromatic moiety of ATP (Fig. 5). In fact, when one examines more closely the predicted interactions performed by both compounds (Fig. 6), the hydrophobic interactions at the terminal phenyl ring of **25a** are reinforced by H bonds with the contiguous sulfonyl group. This seems coherent with the results from the biological assays that suggests **25a** is the most promising compound we have synthesized, probably due to this chemical feature. Furthermore, despite the similar positioning between the pyrrole of ulixertinib (Fig. 6A) and the triazole of **25a** (Fig. 6B), which indicates equivalent cation-π (Lys^{52}) and π-π interaction (Tyr^{34}) for both groups, **25a** would stand out because of an additional π-π interaction of the benzyl group. This connects the triazole and arylsulfonyl group with (Tyr^{34}) and potentially contributes to a stronger interaction profile for the central moiety of this compound. Finally, despite the similar hydrophobic interactions performed with Tyr^{34} and Arg^{65} in both compounds, neither the amide nor the hydroxyl group of the ulixertinib seems to be involved in H-bonding, as observed for the 4-quinazolinamine moiety of **25a**. Once again, the compound we have synthesized seems to explore more efficiently the ERK amino acid residues that are contiguous to the ATP binding cleft than ulixertinib. Accordingly, we decided to compare their potential toxicities and pharmacokinetic profiles (Table 2) to check if **25a** could be (or not) considered a promising lead compound using MetaDrug module of MetaCore platforms from Clarivate Analytics.

Except for the predictions of CYP2C9 and CYP3A4 inhibition by ulixertinib, both compounds did not achieve high similarity levels (Tanimoto Prioritization - TP values) with the compounds in the training sets used to compose the ADMETox QSAR models and, accordingly, the results in Table 2 must be viewed with some caution. In this context, both compounds did not display any relevant toxicity, a fact that agrees with the Phase I dose-escalation study published for ulixertinib, as the observed significant side effects were diarrhea, fatigue, nausea, and dermatitis [11].

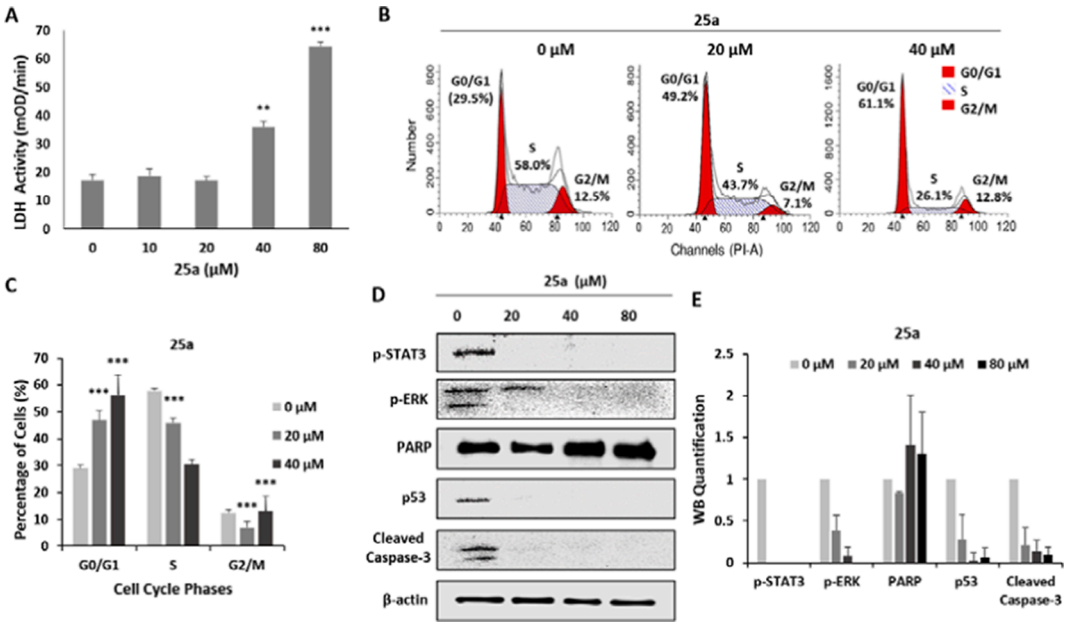

Fig. 4. Effect of compound **25a** on LDH release, cell cycle progression and tumor signaling proteins. **(A) LDH activity assay;** BT-20 cells were treated with **25a** compound at the indicated concentrations for 48 h, and the activity of LDH in the culture medium was measured spectrophotometrically. **(B) Cell cycle distribution analysis;** the cell population histograms in respect to propidium iodide (PI) fluorescence intensity determined by flow cytometry are representative from 3 independent experiments performed in triplicate. BT-20 cells treated with **25a** at the indicated concentrations for 24 h were collected, fixed in 70% cold ethanol, stained with PI, and analysed by flow cytometry. The percentage of cells in different phases of cell cycle are showed for each condition. **(C) Cell cycle distribution analysis;** the graph represents the percentages (mean ± SD) of cells distributed in each cell cycle phase of 3 independent experiments performed in triplicate by flow cytometry. **(D) Signaling proteins**; Total protein from BT-20 cells treated with **25a** for 48 h were extracted and subjected to Western blot analysis of the levels of p-STAT3, p-ERK, PARP, p53 and cleaved caspase-3. β-actin was used as a loading control. **(E) Protein quantification**; the graph represents densitometry of the protein bands of 2 independent experiments. Relative intensity of each target protein band was divided by intensity of the β-actin band, and then the values were compared to the control (0 μM).

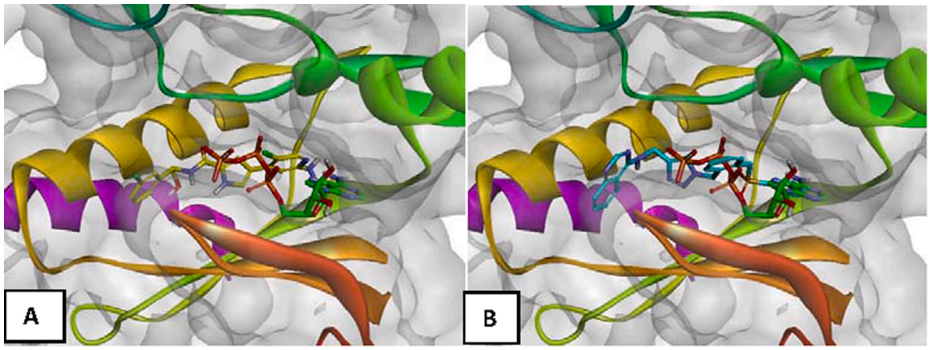

Fig. 5. Proposed binding modes for ulixertinib (**A**, in yellow) and **25a** (**B**, in cyan) at the catalytic cleft of ERK (PDB ID 6DCG). The crystallographic pose of the adenosine triphosphate (in green, recovered from the ERK complex PDB ID 4GT3) was used as a reference for the docked ligands in both panels. (For interpretation of the references to colour in this figure legend, the reader is referred to the web version of this article.)

Concerning the Cytochrome P450 metabolic stability, ulixertinib displays a slightly superior profile because of the expected stability against the 2D6 isoform and, accordingly, **25a** could display relevant drug-drug interactions with known CYP2D6 inhibitors such as bupropion, fluoxetine, paroxetine and terbinafine [62]. As depicted in Fig. 7, the first pass metabolism of **25a** is restricted to Phase 1 aromatic hydroxylation reactions and, particularly, to Phase 2 *N*-conjugations with glucuronide or sulfate. The metabolites of ulixertinib were recently described and involve both *N*-dealkylation or hydroxylation of the terminal carbon of the isopropyl side chain to subsequently yield a carboxylic acid, the direct conjugation with glucuronide at the free hydroxyl group (both for the parent drug or the *N*-dealkylated form) and the aromatic hydroxylation at different positions of the phenyl ring [63].

Unlike ulixertinib, **25a** is not likely to cross the blood brain barrier, which hampers the treatment of CNS tumors. However, as both ulixertinib and **25a** display adequate LogP values, the most interesting optimization achieved for the compound we synthesized is the water solubility. Despite it being below the ideal range ($2 < \text{LogWsol}_{25°C} < 4$ mg/L) [64], its predicted water solubility is more satisfactory than the one for ulixertinib.

3. Conclusion

We have synthesised a small library of triazoles tethered to 4-aminoquinazoline using a Click Chemistry strategy. Initial screening on tumour cells enabled us to identify compound **25a** (IC_{50} 24.6 μM) as the most potent from the series towards BT-20 cells. Despite the promotion of lactate dehydrogenase (LDH) release linking the mode of action to

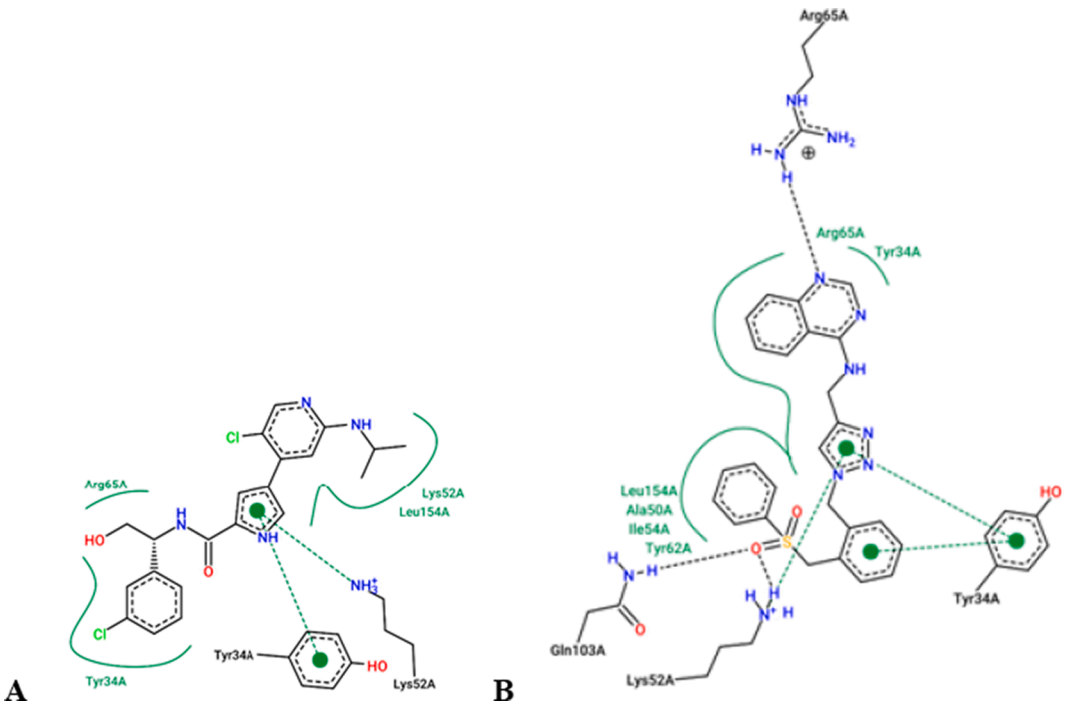

Fig. 6. Two-dimensional diagrams for the docked ligand–ERK interactions generated from 3-D models using PoseView [61]. **(A)** Ulixertinib and **(B) 25a**. Dashed black lines correspond to hydrogen bonds, green dashed lines to π-π or cation-π interactions and the solid green to hydrophobic interactions. (For interpretation of the references to colour in this figure legend, the reader is referred to the web version of this article.)

Table 2
Predicted toxicities and pharmacokinetic parameters for ulixertinib and **25a**. ADME = absorption, distribution, metabolism, and excretion; QSAR = Quantitative structure–activity relationship and TP = Tanimoto Prioritization.

ADME/Toxicity endpoint	Ulixertinib		25a		Threshold
	QSAR value	TP value	QSAR value	TP value	
BBB penetration	−0.64	36.99	−0.28	33.54	>−0.30
CYP2C9 inhibition	0.51	50.62	0.57	48.85	>0.50
CYP2D6 inhibition	0.42	46.88	0.59	48.85	>0.50
CYP3A4 inhibition	0.66	50.62	0.64	48.85	>0.50
hERG inhibition	0.20	37.90	0.35	36.36	> −1.70
LogP	3.15	–	2.92	–	−0.4 to 5.6
Pgp inhibition	−0.43	42.16	−0.76	37.54	>−1.70
Serum protein binding	88.27	36.99	89.15	33.54	>95%
Water solubility	0.17	–	1.47	–	2–4
Carcinogenicity	0.12	42.39	0.34	37.07	>0.50
Cardiotoxicity	0.35	40.53	0.25	34.42	>0.50
Hepatotoxicity	0.19	44.49	0.21	44.49	>0.50
Mutagenicity	0.22	36.01	0.43	37.07	>0.50
Nephrotoxicity	0.17	44.86	0.23	38.82	>0.50
Neurotoxicity	0.09	42.57	0.25	38.22	>0.50

necrosis, compound **25a** was able to induce, in a dose-dependent manner, an increase in the subpopulation of cells in G0/G1 in parallel to the decrease in S phase of BT-20 cells. Taking into account the essential role of p-ERK1/2 and p-STA3 in the positive regulation of G1 to S phase progression, we incubated BT-20 cells with **25a** and analysed proteins related to tumour cell signalling by Western blot assays. The significant p-ERK1/2 and p-STA3 kinases decrease led us to infer their possible inhibition as the main mechanism underlying the **25a**-induced cell cycle arrest. Inspired by the importance of p-ERK1/2 as therapeutic target for breast cancer treatment, we performed docking studies to predict the binding mode of compound **25a** at ATP binding cleft and concluded that it could bind more efficiently than ulixertinib, a drug

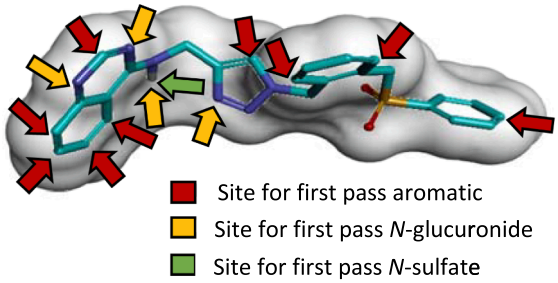

Fig. 7. Main predicted sites for first pass Phase 1 and 2 metabolic reactions in **25a**.

under clinical evaluation. *In silico* pharmacokinetics data strengthens compound **25a** as an interesting pharmacological probe for further investigations.

4. Experimental section

4.1. Chemistry

Reagents and solvents were commercially obtained as reagent grade and used without any purification (Merck® and TEDIA® respectively). The reaction progress and separation were monitored by thin layer chromatography and the spots were visualized using ultraviolet light (UV − 254 nm). Flash chromatography equipment Biotage Isolera was used for purification using normal phase cartridges. NMR analysis were obtained on a Bruker Advance spectrometer at 300, 400 or 500 MHz. A Bruker Daltonics micrOTOF-Q II™ ESI-Qq-TOF mass spectrometer was used to perform High Resolution Mass Spectroscopy (HRMS) analysis.

Compounds **24a,b, 26a and 27a** were obtained according to described procedures [30,31] and the novel compounds were obtained via Copper-catalysed Azide-Alkyne Cycloaddition (CuAAC) reactions [29,42]. Non-commercial starting materials, obtained from previously

described protocols, are briefly reported in the supplementary information.

General procedure A – To a microwave flask containing a magnetic stirring bar, sodium ascorbate (0.2 eq.) diluted with DMF (100 μL) was added followed by $CuSO_4$ (0.05 eq., 1 mol.L^{-1} in water). The reaction mixture was stirred for 5 min and then the alkyne derivative (**6a-c**, 1.1 eq.) and azido derivative (**7–13,** 1 eq.), both diluted in DMF, were added. The reaction mixture was microwaved with 100 W, 80 °C for 5–10 min. The crude reaction was poured in EtOAc and extracted with brine. The organic phase was concentrated and purified by flash chromatography (EtOAc/MeOH 5%).

*4.1.1. N-[(1-benzyl-1H-1,2,3-triazol-4-yl)methyl]quinazolin-4-amine **(21a)***

Yield: 67% (53 mg, 0.17 mmol). ^{1}H NMR (300 MHz, $DMSO_{d6}$) δ_H (ppm): 8.77 (1H, t, *J* 5.6 Hz, H-9), 8.44 (1H, s, H-7), 8.20 (1H, d, *J* 7.8 Hz, H-3), 8.02 (1H, s, H-12), 7.79–7.60 (2H, m, H-2, H-6), 7.47 (1H, ddd, *J* 8.2 Hz, *J* 6.9 Hz, *J* 1.3 Hz, H-1), 7.36–7.21 (5H, m, H-Ar), 5.49 (2H, s, H-13), 4.75 (2H, d, *J* 5.7 Hz, H-10). ^{13}C NMR (75 MHz, $DMSO_{d6}$) δ_C (ppm): 159.2 (C-8), 155.0 (C-7), 149.1 (C-4), 145.2 (C-11), 136.2 (C-14), 132.7 (C-2), 128.7 (C-17, C-18), 128.1 (C-19), 128.0 (C-15, C-16), 127.5 (C-6), 125.8 (C-1), 123.3 (C-12), 122.7 (C-3), 115.0 (C-5), 52.7 (C-13), 36.0 (C-10). HRMS (ES^+): *m/z* $[M+H]^+$ calculated for $C_{18}H_{17}N_6^+$: 317.1509, found: 317.1508.

*4.1.2. N-{[1-(4-nitrobenzyl)-1H-1,2,3-triazol-4-yl] methyl} quinazolin-4-amine **(22a)***

Yield: 42% (38 mg, 0.10 mmol). ^{1}H NMR (500 MHz, $DMSO_{d6}$) δ_H (ppm): 8.84 (1H, t, H-9), 8.50 (1H, s, H-7), 8.25 (1H, d, *J* 8.3 Hz, H-3), 8.21 (2H, d, *J* 8.7 Hz, H-17, H-18), 8.15 (1H, s, H-12), 7.77 (1H, t, *J* 7.6 Hz, H-2), 7.70 (1H, d, *J* 8.3 Hz, H-6), 7.54–7.48 (3H, m, H-1, H-15, H-16), 5.73 (2H, s, H-13), 4.82 (4H, d, *J* 5.6 Hz, H-10). ^{13}C NMR (126 MHz, $DMSO_{d6}$) δ_C (ppm): 159.1 (C-8), 154.9 (C-7), 149.0 (C-4), 147.2 (C-19), 145.3 (C-11), 143.4 (C-14), 132.5 (C-2), 128.9 (C-15, C-16), 127.4 (C-6), 125.6 (C-1), 123.7 (C-17, C-18), 123.6 (C-12), 122.6, (C-3), 114.9 (C-5), 51.7 (C-13), 35.9 (C-10). HRMS (ES^+): *m/z* $[M+H]^+$ calculated for $C_{18}H_{16}N_7O_2^+$: 362.1360, found: 362.1360.

*4.1.3. N-{[1-(4-methoxybenzyl)-1H-1,2,3-triazol-4-yl]methyl}quinazolin-4-amine **(23a)***

Yield: 53% (17 mg, 0.049 mmol). ^{1}H NMR (400 MHz, $CDCl_3$) δ_H (ppm): 8.65 (1H, s, H-7), 7.86–7.76 (2H, m,H-3, H-6), 7.72 (1H, t, *J* 8.3 Hz, H-2), 7.55 (1H, s, H-12), 7.43 (1H, t, *J* 8.2 Hz, H-1), 7.27–7.21 (2H, m, H-15, H-16), 6.97 (1H, sl, H-9), 6.91–6.87 (2H, m, H-17, H-18), 5.45 (2H, s, H-13), 4.90 (2H, d, *J* 5.0 Hz, H-10), 3.80 (3H, s, H-20). ^{13}C NMR (101 MHz, $CDCl_3$) δ_C (ppm): 160.2 (C-8), 159.3 (C-19), 155.0 (C-7), 149.1 (C-4), 144.9 (C-11), 132.9 (C-2), 129.8 (C-15, C-16), 128.3 (C-3), 126.4 (C-1), 126.5 (C-14), 122.3 (C-12), 121.1 (C-6), 115.1 (C-5), 114.7 (C-17, C-18), 55.5 (C-20), 54.0 (C-13), 36.6 (C-10). HRMS (ES^+): *m/z* $[M+H]^+$ calculated for $C_{19}H_{19}N_6O^+$: 347.1615, found: 347.1616.

*4.1.4. N-{[1-(2-((phenylsulfonyl)methyl]benzyl}-[(1H-1,2,3-triazol-4-yl) methyl] quinazolin-4-amine **(25a)***

Yield: 65% (16 mg, 0.034 mmol). ^{1}H NMR (500 MHz, $DMSO_{d6}$) δ_H (ppm): 8.81 (1H, t, *J* 5.6 Hz, H-9), 8.47 (1H, s, H-7), 8.22 (1H, d, *J* 8.2 Hz, H-3), 8.00 (1H, s, H-12), 7.79 (2H, d, *J* 8.1 Hz, H-22, H-26), 7.75 (2H, t, *J* 7.5 Hz, H-23, H-25), 7.69 (1H, d, *J* 8.3 Hz, H-6), 7.62 (2H, t, *J* 7.8 Hz, H-2, H-24), 7.50 (1H, t, *J* 7.6 Hz, H-1), 7.31 (1H, t, *J* 7.5 Hz, H-19), 7.23 (1H, d, *J* 7.6 Hz, H-17), 7.08 (2H, t, *J* 7.3 Hz, H-16, H-18), 5.60 (2H, s, H-13), 4.91 (2H, s, H-20), 4.78 (2H, d, *J* 5.6 Hz, H-10). ^{13}C NMR (126 MHz; $DMSO_{d6}$) δ_C (ppm): 159.1 (C-8), 154.9 (C-7), 149.0 (C-4), 145.3 (C-11), 138.4 (C-15), 136.5 (C-14), 134.1 (C-24), 133.0 (C-16), 132.6 (C-2), 129.3 (C-23, C-25), 129.2 (C-17), 128.8 (C-18), 128.1 (C-22, C-26), 128.0 (C-19), 127.4 (C-6), 126.6 (C-21), 125.7 (C-1), 123.4 (C-12), 122.7 (C-3), 114.9 (C-5), 57.8 (C-20), 49.9 (C-13), 35.9 (C-10). HRMS (ES^+): *m/z* $[M+H]^+$ calculated for $C_{25}H_{23}N_6O_2S^+$: 471.1598, found: 471.1599.

*4.1.5. N-[(1-benzyl-1H-1,2,3-triazol-4-yl)methyl]-6,7-dimethoxyquinazolin-4-amine **(21b)***

Yield: 72% (51 mg, 0.13 mmol). ^{1}H NMR (300 MHz, $CDCl_3$) δ_H (ppm): 8.53 (1H, s, H-7), 7.65 (1H, s, H-12), 7.38 (3H, dd, *J* 5.0 Hz, *J* 1.8 Hz, H-Ar), 7.28 (2H, d, *J* 7.7 Hz, H-Ar), 7.15 (1H, s, H-3), 7.03 (2H, s, H-6, H-9), 5.50 (2H, s, H-13), 4.89 (2H, d, *J* 5.4 Hz, H-10), 3.99 (3H, s, H-20), 3.79 (3H, s, H-21).^{13}C NMR (75 MHz, $CDCl_3$) δ_C (ppm): 158.1 (C-2), 154.4 (C-8), 153.8 (C-7), 149.0 (C-1), 146.5 (C-4), 134.5 (C-14), 129.3 (C-15, C-16), 129.0 (C-19), 128.2 (C-17, C-18), 122.9 (C-12), 107.5 (C-3), 100.1 (C-6), 56.3 (C-21), 56.2 (C-20), 54.5 (C-13), 36.3 (C-10). HRMS (ES^+): *m/z* $[M+H]^+$ calculated for $C_{20}H_{21}N_6O_2^+$: 377.1721, found: 377.1719.

*4.1.6. 6,7-dimethoxy-N-{[1-(4-nitrobenzyl)-1H-1,2,3-triazol-4-yl]methyl} quinazolin-4-amine **(22b)***

Yield: 45% (36 mg, 0.08 mmol). ^{1}H NMR (300 MHz, $DMSO_{d6}$) δ_H (ppm): 8.49 (2H, t, *J* 5.4 Hz, H-7, H-9), 8.22 (2H, d, *J* 8.5 Hz, H-17, H-18), 8.14 (1H, s, H-12), 7.63 (1H, s, H-6), 7.51 (2H, d, *J* 8.6 Hz, H-17, H-18), 7.12 (1H, s, H-3), 5.73 (2H, s, H-13), 4.79 (2H, d, *J* 5.4 Hz. H-10), 3.89 (3H, s, H-20), 3.86 (3H, s, H-21).^{13}C NMR (126 MHz, $DMSO_{d6}$) δ_C (ppm): 157.9 (C-2), 153.8 (C-8), 153.2 (C-7), 148.3 (C-1), 147.2 (C-19), 145.6 (C-14), 143.4 (C-4), 129.0 (C-17, C-18), 123.8 (C-15, C-16), 123.6 (C-12), 107.0 (C-3), 102.0 (C-6), 55.9 (C-20), 55.6 (C-21), 51.7 (C-13), 35.7 (C-10). HRMS (ES^+): *m/z* $[M+H]^+$ calculated for $C_{20}H_{20}N_7O_4^+$: 422.1577, found: 422.1574.

*4.1.7. 6-(benzyloxy)-7-methoxy-N-{[1-(4-nitrobenzyl)-1H-1,2,3-triazol-4-yl]methyl} quinazolin-4-amine **(22c)***

A mixture of $CuSO_4$ (0.45 mg, 0.003 mmol, 5 mol%), 1,10-phenantroline monohydrate (0.5 mg, 0.003 mmol, 5 mol%), and sodium ascorbate (11 mg, 0.06 mmol) in EtOH:H_2O [2:1 (v/v), 1 mL], was stirred for 5 min at room temperature. Subsequently the compounds 4-amino-[*N*- (propynyl)]-6-benzyloxy-7-methoxy-quinazoline **(6c)** (19.7 mg, 0.06 mmol) and 1-(azidomethyl)-4-nitro-benzene **(8)** (10 mg, 0.06 mmol) diluted in EtOH:H_2O [2:1 (v/v); 1 mL] were added to the reaction mixture, which was stirred for 18 h at room temperature. After, the reaction mixture was concentrated in vacuo and purified by silica gel column chromatography [EtOAc: MeOH (9.5:0.5)]. The compound **22c** was obtained in quantitative yield (28 mg, 0.06 mmol).^{1}H NMR (300 MHz, $DMSO_{d6}$) δ_H (ppm): δ 8.49 (1H, d, *J* 5.5 Hz, H-9), 8.39 (1H, s, H-7), 8.22 (2H, d, *J* 8.8 Hz, H-17, H-18), 8.15 (1H, s, H-12), 7.81 (1H, s, H-6), 7.55–7.47 (4H, m, H-15, H-16, H-22, H-26), 7.46–7.32 (3H, m, H-23, H-24, H-25), 7.13 (1H, s, H-3), 5.74 (2H, s, H-13), 5.13 (2H, s, H-21), 4.81 (2H, d, *J* 5.4 Hz, H-10), 3.89 (3H, s, H-20).^{13}C NMR (75 MHz, $DMSO_{d6}$) δ_C (ppm): 158.1 (C-8), 154.0 (C-2), 153.5 (C-7), 147.4 (C-1), 147.2 (C-4), 146.1 (C-19), 145.6 (C-14), 143.6 (C-27), 136.4 (C-11), 129.1 (C-15, C-16), 128.6 (C-23, C-25), 128.3 (C-22, C-26), 128.2 (C-24), 123.9 (C-17, C-18), 123.8 (C-12), 108.5 (C-5), 107.1 (C-3), 103.3 (C-6), 70.4 (C-21), 55.8 (C-20), 51.8 (C-13), 35.8 (C-10).HRMS (ES^+): *m/z* $[M+H]^+$ calculated for $C_{26}H_{24}N_7O_4^+$ 498.1884, found: 498.1881.

*4.1.8. 7-methoxy-4-{[1-(4-nitrobenzyl)-1H-1,2,3-triazol-4-yl] methylamino}quinazolin-6-ol **(22d)***

A solution of compound **22c** (10 mg, 0.02 mmol) in TFA (110 μL) was refluxed for 50 min. After cooling to room temperature the mixture was poured into ice. The solvent was removed in vacuo and the crude product was purified by filtration over Discovery® DSC-18 SPE cartridge (H_2O:MeOH). Yield: 55% (4.5 mg, 0.01 mmol). ^{1}H NMR (300 MHz, CD_3OD) δ_H (ppm): 8.64 (1H, s, H-7), 8.23 (2H, d, *J* 8.8 Hz, H-17, H-18), 8.12 (1H, s, H-12), 7.59 (1H, s, H-3), 7.51 (2H, d, *J* 8.8 Hz, H-15, H-16), 7.16 (1H, s, H-6), 5.74 (2H, s, H-13), 5.04 (2H, s, H-10), 4.08 (3H, s, H-21). ^{13}C NMR (101 MHz, CD_3OD) δ_C (ppm): 161.2 (C-8), 157.6 (C-2), 150.4 (C-1), 149.4 (C-7), 149.3 (C-4), 143.9 (C-19), 134.9 (C-11), 130.0 (C-15, C-16), 125.3 (C-12), 125.0 (C-17, C-18), 109.0 (C-5), 107.3 (C-3),

100.3 (C-6), 57.3 (C-21), 53.9 (C-13), 37.9 (C-10). HRMS (ES^+): *m/z* $[M+H]^+$ calculated for $C_{19}H_{18}N_7O_4^+$ 408.1415, found: 408.1412.

4.1.9. 6,7-dimethoxy-N-{[1-(4-methoxybenzyl)-1H-1,2,3-triazol-4-yl] methyl}quinazolin-4-amine (**23b**)

Yield: 55% (42 mg, 0.10 mmol). ^1H NMR (300 MHz, $DMSO_{d6}$) δ_H (ppm): 9.93 (1H, t, *J* 4.4 Hz, H-9), 8.59 (1H, s, H-7), 7.88 (1H, s, H-12), 7.60 (1H, s, H-6), 7.03 (2H, d, *J* 8.6 Hz, H-15, H-16), 6.97 (1H, s, H-3), 6.65 (2H, d, *J* 8.6 Hz, H-17, H-18), 5.22 (2H, s, H-13), 4.69 (2H, d, *J* 5.4 Hz, H-10), 3.70 (3H, s, H-21), 3.64 (3H, s, H-22), 3.46 (3H, s, H-20). ^{13}C NMR (101 MHz, $DMSO_{d6}$) δ_C (ppm): 159.2 (C-2), 156.1 (C-19), 150.1 (C-8), 149.1 (C-7), 143.3 (C-1), 134.3 (C-11), 129.8 (C-15, C-16), 127.9 (C-14), 123.4 (C-12), 114.2 (C-17, C-18), 106.6 (C-5), 103.3 (C-3), 99.6 (C-6), 56.5 (C-21, C-22), 55.2 (C-20), 52.5 (C-13), 36.8 (C-10). HRMS (ES^+): *m/z* $[M+H]^+$ calculated for $C_{21}H_{23}N_6O_3^+$: 407.1826, found: 407.1825.

4.2. Cell culture

The breast carcinoma cell line BT-20 (ATCC® HTB-19™), tongue squamous cell carcinoma HN13 [65] and Cal-27 (ATCC CRL-2095), gastric carcinoma HGC-27 (BCRJ), and normal fibroblast [66] were grown in Dulbecco's Modified Eagle Medium (DMEM, Sigma, St. Louis, MO, USA) supplemented with 10% fetal bovine serum, 100 U/mL penicillin and 100 μg/mL streptomycin. The cultures were maintained in a humidified 5% CO_2 atmosphere at 37 °C.

4.3. Cell viability

The resazurin assay was used to determine cell viability. The cells were seeded on 96-well plates (4,000 cells/well) and treated with compounds at different concentrations for 48 h. After treatment, the medium was replaced by DMEM phenol red-free (Sigma-Aldrich) containing resazurin (0.01 $mg.mL^{-1}$ dissolved in PBS; Sigma-Aldrich), and the plates incubated in the dark for 4 h at 37 °C. Finally, cell viability was measured by detection of fluorescence in a microplate fluorimeter (excitation 530/25 nm, emission 590/35 nm). Three independent biological experiments were performed in quadruplicate. The data were plotted and the IC_{50} value was estimated by nonlinear regression. Cell viability was also assessed using the lactate dehydrogenase (LDH) assay (Sigma-Aldrich) to measure the activity of LDH released in the cell culture medium as an indicator of necrosis. The cells were seeded on 24-well plates (50,000 cells/well). After 24 h, cells were treated with compounds at different concentrations in DMEM phenol red-free at 37 °C in 5% CO_2 for 48 h. Next, the supernatant was transferred to a new plate and the LDH reaction mix added. After incubation for 30 min at room temp, the LDH activity was quantified by a microplate reader at OD450nm.

4.4. Cell cycle analysis

BT-20 cells were seeded on 6-well plates (3×10^5 cells/well) and then incubated with **25a** for 24 h. Next, cells were collected and fixed in 70% cold ethanol for 1 h, treated with RNase (100 $\mu g.mL^{-1}$) for 30 min at 37 °C and stained with propidium iodide (50 $\mu g.mL^{-1}$) for 15 min at 37 °C. Next, cell subpopulations in each cell cycle phase were determined by using FACSCalibur flow cytometry (BD Biosciences - San Jose, CA, USA). The cell cycle distribution was analysed using ModFit LT V3-0.3.11 software.

4.5. Western blot

BT-20 cells were cultured in 6-well plates (3×10^5 cells/well), followed by incubation with the compound **25a** (20 and 40 μM) in serum-free medium for 48 h. Next, cells were harvested in CelLytic MT buffer (Sigma-Aldrich) supplemented with phosphatases and proteases inhibitors (Sigma-Aldrich), subjected to sonication (three times at 5 s each) and the cell lysate was centrifuged at 13,000*g* for 15 min at 4 °C. The supernatant was collected, and protein concentration was determined by using Bradford protein assay (BioRad). Total proteins (30 μg) were separated in 10% SDS-PAGE gel and transferred onto nitrocellulose membranes. The protein marker ladder (Spectra multicolour broad range protein ladder, Thermo Scientific) was included in all gels. Membranes were incubated overnight at 4 °C with primary antibodies for p-STAT3 (#9145), p-ERK1/2 (#4377), p53 (#2527), PARP (#9532) and cleaved caspase-3 (#9661) from Cell Signalling, and β-Actin (sc47778) from Santa Cruz Biotechnology. Then, membranes were washed and incubated with horseradish peroxidase-conjugated secondary antibodies for 1 h at room temperature. Immunocomplexes were detected by chemiluminescence using the ECL Western blotting reagent (GE HealthCare) in a ChemiDoc XRS detection system (BioRad). Densitometric analysis of protein bands by Western blot was performed using ImageJ software. The intensities of the target proteins bands were divided by β-Actin and the value compared to control (0 μM).

4.6. Statistical analyses

The statistical analysis was carried out with Student's t-test or ANOVA. The results were considered statistically significant if * $p < 0.05$, ** $p < 0.01$, and *** $p < 0.001$.

4.7. Molecular modelling

The 3-D ligand structures were built as we previously reported [67], while we have also described the detailed docking procedures elsewhere [68]. Molecular docking simulations were performed using the structure of the mammalian ERK enzyme complexed with the ATP competitive dual ERK1/2 kinase inhibitor MK-8353 (PDB ID 6DCG; complex resolution: 1.45 Å), since both the similarity of MK-8353 (Tanimoto coefficient = 0.32) with **25a** and the complex resolution were slightly greater than the observed for Ulixertinib (PDB ID 6GDQ) (Tanimoto coefficient = 0.29; $Res_{\_6GDQ}$ = 1.86 Å). The choice of the most similar crystallographic compound with the docked ligands tend to improve the accuracy of the simulation results, probably because of ligand-induced fit effects [69]. Redocking of the crystallographic ligand yielded a heavy atom Root Mean Square Deviation (RMSD) of 0.76 Å, while the docking poses were ranked using the GlideScore fitness function [70]. The top-scored docking poses for the ligands were selected for visual inspection and the subsequent analyses of the protein–ligand interactions. The crystallographic pose of ATP (PDB ID 4GT3) was used as a reference in the visual inspection after superposition of the two ERK complexes. Both ulixertinib and the most promising synthesized, **25a**, compound were subjected to subsequent *in silico* analyses using the MetaDrug module of MetaCore platforms from Clarivate Analytics to predict their potential toxicities and pharmacokinetic profiles.

Declaration of Competing Interest

The authors declare that they have no known competing financial interests or personal relationships that could have appeared to influence the work reported in this paper.

Acknowledgments

This work was supported by Fundação de Amparo à Pesquisa do Estado de São Paulo-FAPESP, Brazil (Grants 2015/07893-6, 2013/27186-7, 2018/17480-9, 2018/08585-1), and Conselho Nacional de Desenvolvimento Científico e Tecnológico-CNPq, Brazil (Grants 308521/2017-0, 301560/2018-8).

Appendix A. Supplementary material

Supplementary data to this article can be found online at https://doi.org/10.1016/j.bioorg.2021.104982.

References

[1] F. Bray, J. Ferlay, I. Soerjomataram, R.L. Siegel, L.A. Torre, A. Jemal, Global cancer statistics 2018: GLOBOCAN estimates of incidence and mortality worldwide for 36 cancers in 185 countries, CA Cancer J. Clin. 68 (2018) 394-424. http://dx.doi.10.3322/caac.21492.

[2] M. Sciacovelli, C. Schmidt, E.R. Maher, C. Frezza, Metabolic Drivers in Hereditary Cancer Syndromes, Annu. Rev. Cancer Biol. 4 (2020) 77–97, https://doi.org/10.1146/annurev-cancerbio-030419-033612.

[3] J. Birnbaum, V.K. Gadi, E. Markowitz, R. Etzioni, The Effect of Treatment Advances on the Mortality Results of Breast Cancer Screening Trials: A Microsimulation Model, Ann. Intern. Med. 164 (2016) 236–243, https://doi.org/10.7326/M15-0754.

[4] E. Fleuren, L. Zhang, J. Wu, R.J. Daly, The kinome 'at large' in cancer, Nat. Rev. Cancer 16 (2016) 83–98, https://doi.org/10.1038/nrc.2015.18.

[5] R. Roskoski Jr., Properties of FDA-approved small molecule protein kinase inhibitors: A 2020 update, Pharmacol. Res. 152 (2020), 104609, https://doi.org/10.1016/j.phrs.2019.104609.

[6] F.M. Ferguson, N.S. Gray, Kinase inhibitors: the road ahead, Nat. Rev. Drug. Discov. 17 (2018) 353–377, https://doi.org/10.1038/nrd.2018.21.

[7] R. Yaeger, R.B. Corcoran, Targeting Alterations in the RAF-MEK Pathway, Cancer Discov. 9 (2019) 329–341, https://doi.org/10.1158/2159-8290.CD-18-1321.

[8] C.R. Lindsay, F.H. Blackhall, Direct Ras G12C inhibitors: crossing the rubicon, Br. J. Cancer 121 (2019) 197–198, https://doi.org/10.1038/s41416-019-0499-1.

[9] Z. Karoulia, E. Gavathiotis, P.I. Poulikakos, New perspectives for targeting RAF kinase in human cancer, Nat. Rev. Cancer 17 (2017) 676–691, https://doi.org/10.1038/nrc.2017.79.

[10] Y. Zhao, A.A. Adjei, The clinical development of MEK inhibitors, Nat. Rev. Clin. Oncol. 11 (2014) 385–400, https://doi.org/10.1038/nrclinonc.2014.83.

[11] R.J. Sullivan, J.R. Infante, F. Janku, D.J.L. Wong, J.A. Sosman, V. Keedy, M. R. Patel, G.I. Shapiro, J.W. Mier, A.W. Tolcher, A. Wang-Gillam, M. Sznol, K. Flaherty, E. Buchbinder, R.D. Carvajal, A.M. Varghese, M.E. Lacouture, A. Ribas, S.P. Patel, G.A. Decrescenzo, C.M. Emery, A.L. Groover, S. Saha, M. Varterasian, D. J. Welsch, D.M. Hyman, B.T. Li, First-in-class ERK1/2 Inhibitor Ulixertinib (BVD-523) in patients with MAPK mutant advanced solid tumors: results of a Phase I dose-escalation and expansion study, Cancer Discov. 8 (2018) 184–195, https://doi.org/10.1158/2159-8290.CD-17-1119.

[12] J.N. Sanchez, T. Wang, M.S. Cohen, BRAF and MEK Inhibitors: Use and Resistance in BRAF-Mutated Cancers, Drugs 78 (2018) 549–566, https://doi.org/10.1007/s40265-018-0884-8.

[13] S. Saha, D. Welsch, G. DeCrescenzo, J.J. Roix. US 20160317519 A1, 2016.

[14] S.B. Boga, Y. Deng, L. Zhu, Y. Nan, A.B. Cooper, G.W. Shipps-Jr, R. Doll, N.-Y. Shih, H. Zhu, R. Sun, T. Wang, S. Paliwal, H.-C. Tsui, X. Gao, X. Yao, J. Desai, J. Wang, A. B. Alhassan, J. Kelly, M. Patel, K. Muppalla, S. Gudipati, L.-K. Zhang, A. Buevich, D. Hesk, D. Carr, P. Dayananth, S. Black, H. Mei, K. Cox, B. Sherborne, A.W. Hruza, L. Xiao, W. Jin, B. Long, G. Liu, S.A. Taylor, P. Kirschmeier, W.T. Windsor, R. Bishop, A.A. Samatar, MK-8353: Discovery of an Orally Bioavailable Dual Mechanism ERK Inhibitor for Oncology, ACS Med, Chem. Lett. 9 (2018) 761–767, https://doi.org/10.1021/acsmedchemlett.8b00220.

[15] E.J. Morris, S. Jha, C.R. Restaino, P. Dayananth, H. Zhu, A. Cooper, D. Carr, Y. Deng, W. Jin, S. Black, B. Long, J. Liu, E. DiNunzio, W. Windsor, R. Zhang, S. Zhao, M.H. Angagaw, E.M. Pinheiro, J. Desai, L. Xiao, G. Shipps, A. Hruza, J. Wang, J. Kelly, S. Paliwal, X. Gao, B.S. Babu, L. Zhu, P. Daublain, L. Zhang, B. A. Lutterbach, M.R. Pelletier, U. Philippar, P. Siliphaivanh, D. Witter, P. Kirschmeier, W.R. Bishop, D. Hicklin, D.G. Gilliland, L. Jayaraman, L. Zawel, S. Fawell, A.A. Samatar, Discovery of a novel ERK inhibitor with activity in models of acquired resistance to BRAF and MEK inhibitors, Cancer Discov. 3 (2013) 742–750, https://doi.org/10.1158/2159-8290.CD-13-0070.

[16] S.J. Moschos, R.J. Sullivan, W.-J. Hwu, R.K. Ramanathan, A.A. Adjei, P.C. Fong, R. Shapira-Frommer, H.A. Tawbi, J. Rubino, T.S. Rush III, D. Zhang, N.R. Miselis, A.A. Samatar, P. Chun, E.H. Rubin, J. Schiller, B.J. Long, P. Dayananth, D. Carr, P. Kirschmeier, W. Robert Bishop, Y. Deng, A. Cooper, G.W. Shipps, B.H. Moreno, L. Robert, A. Ribas, K.T. Flaherty. Development of MK-8353, an orally administered ERK1/2 inhibitor, in patients with advanced solid tumors, JCI Insight, 3 (2018) e92352. http://dx.doi.10.1172.jci.insight.92352.

[17] D.J. Burdick, S. Wang, C. Heise, B. Pan, J. Drummond, J.P. Yin, L. Goeser, S. Magnuson, J. Blaney, J. Moffat, W. Wang, H. Chen, Fragment-based discovery of potent ERK2 pyrrolopyrazine inhibitors, Bioorg. Med. Chem. Lett. 25 (2015) 4728–4732, https://doi.org/10.1016/j.bmcl.2015.08.048.

[18] A.M. Kidger, J. Sipthorp, S.J. Cook, ERK1/2 inhibitors: New weapons to inhibit the RAS-regulated RAF-MEK1/2-ERK1/2 pathway, Pharmacol. Ther. 187 (2018) 45–60, https://doi.org/10.1016/j.pharmthera.2018.02.007.

[19] P.A. Schwartz, P. Kuzmic, J. Solowiej, S. Bergqvist, B. Bolanos, C. Almaden, A. Nagata, K. Ryan, J. Feng, D. Dalvie, J.C. Kath, M. Xu, R. Wani, B.W. Murray, Covalent EGFR inhibitor analysis reveals importance of reversible interactions to potency and mechanisms of drug resistance, PNAS 111 (2014) 173–178, https://doi.org/10.1073/pnas.1313733111.

[20] S. Marchetti, D. Pluim, M. van Eijndhoven, O. van Tellingen, R. Mazzanti, J. H. Beijnen, J.H.M. Schellens, Effect of the drug transporters ABCG2, Abcg2, ABCB1 and ABCC2 on the disposition, brain accumulation and myelotoxicity of the aurora kinase B inhibitor barasertib and its more active form barasertib-hydroxy-QPA, Invest. New Drugs 31 (2013) 1125–1135, https://doi.org/10.1007/s10637-013-9923-1.

[21] D. Das, J. Hong, Recent advancements of 4-aminoquinazoline derivatives as kinase inhibitors and their applications in medicinal chemistry, Eur. J. Med. Chem. 170 (2019) 55–72, https://doi.org/10.1016/j.ejmech.2019.03.004.

[22] J.J. Caldwell, E.J. Welsh, C. Matijssen, V.E. Anderson, L. Antoni, K. Boxall, F. Urban, A. Hayes, F.I. Raynaud, L.J.M. Rigoreau, T. Raynham, G.W. Aherne, L. H. Pearl, A.W. Oliver, M.D. Garrett, I. Collins, Structure-based design of potent and selective 2-(quinazolin-2-yl)phenol inhibitors of checkpoint kinase 2, J. Med. Chem. 54 (2011) 580–590, https://doi.org/10.1021/jm101150b.

[23] A. Azzariti, G. Bocci, L. Porcelli, A. Fioravanti, P. Sini, G.M. Simone, A.E. Quatrale, P. Chiarappa, A. Mangia, S. Sebastian, D. Del Bufalo, M. Del Tacca, A. Paradiso, Aurora B kinase inhibitor AZD1152: determinants of action and ability to enhance chemotherapeutics effectiveness in pancreatic and colon cancer, Br. J. Cancer 104 (2011) 769–780, https://doi.org/10.1038/bjc.2011.21.

[24] R.W. Wilkinson, R. Odedra, S.P. Heaton, S.R. Wedge, N.J. Keen, C. Crafter, J. R. Foster, M.C. Brady, A. Bigley, E. Brown, K.F. Byth, N.C. Barrass, K.E. Mundt, K. M. Foote, N.M. Heron, F.H. Jung, A.A. Mortlock, F.T. Boyle, S. Green, AZD1152, a selective inhibitor of Aurora B kinase, inhibits human tumor xenograft growth by inducing apoptosis, Clin. Cancer Res. 13 (2007) 3682–3688, https://doi.org/10.1158/1078-0432.CCR-06-2979.

[25] G.F. Smith, M.D. Altman, B. Andresen, J. Baker, J.D. Brubaker, H. Chen, Y. Chen, M. Childers, A. Donofrio, H. Ferguson, C. Fischer, T.O. Fischmann, C. Gibeau, A. Hicks, S. Jin, S. Kattar, M.A. Kleinschek, E. Leccese, C. Lesburg, C. Li, J. Lim, D. Liu, J.K.F. Maclean, F. Mansoor, L.Y. Moy, E.F. Mulrooney, A.S. Necheva, J. Presland, L. Rakhilin, R. Yang, L. Torres, J. Zhang-Hoover, A. Northrup, Identification of quinazoline based inhibitors of IRAK4 for the treatment of inflammation, Bioorg. Med. Chem. Lett. 27 (2017) 2721–2726. http://dx.doi.10.1016/j.bmcl.2017.04.050.

[26] A. Nour, T. Hayashi, M. Chan, S. Yao, R.I. Tawatao, B. Crain, I.F. Tsigelny, V. L. Kouznetsova, A. Ahmadiiveli, K. Messer, M. Pu, M. Corr, D.A. Carson, H. B. Cottam, Discovery of substituted 4-aminoquinazolines as selective Toll-like receptor 4 ligands, Bioorg. Med. Chem. Lett. 24 (2014) 4931–4938, https://doi.org/10.1016/j.bmcl.2014.09.039.

[27] Z. Hosseinzadeh, A. Ramazani, N. Razzaghi-Asl, Anti-cancer Nitrogen-Containing Heterocyclic Compounds, Curr. Org. Chem. 22 (2018) 2256–2279, https://doi.org/10.2174/1385272822666181008142138.

[28] D. Fabbro, S.W. Cowan-Jacob, H. Moebitzet, Ten things you should know about protein kinases: IUPHAR Review 14, Br. J. Pharmacol. 172 (2015) 2675–2700, https://doi.org/10.1111/bph.13096.

[29] V. Aragão-Leoneti, V.L. Campo, A.S. Gomes, R.A. Field, I. Carvalho, Application of copper(I)-catalysed azide/alkyne cycloaddition (CuAAC) 'click chemistry' in carbohydrate drug and neoglycopolymer synthesis, Tetrahedron 66 (2010) 9475–9492, https://doi.org/10.1016/j.tet.2010.10.001.

[30] P. de Andrade, S.P. Mantoani, P.S.G. Nunes, C.R. Magadán, C. Pérez, D.J. Xavier, E. T.S. Hojo, N.E. Campillo, A. Martínez, I. Carvalho, Highly potent and selective aryl-1,2,3-triazolyl benzylpiperidine inhibitors toward butyrylcholinesterase in Alzheimer's disease, Bioorg. Med. Chem. 27 (2019) 931–943, https://doi.org/10.1016/j.bmc.2018.12.030.

[31] D.F. Santos, D.R.B. Pilger, C. Vandermeulen, R. Khouri, S.P. Mantoani, P.S. G. Nunes, P. Andrade, I. Carvalho, J. Casseb, J.-C. Twizere, L. Willems, L. Freitas-Jr, S. Kashima, Non-cytotoxic 1,2,3-triazole tethered fused heterocyclic ring derivatives display Tax protein inhibition and impair HTLV-1 infected cells, Bioorg. Med. Chem. 28 (2020), 115746, https://doi.org/10.1016/j.bmc.2020.115746.

[32] F.R. Alexandre, A. Berecibar, T. Besson, Microwave-assisted Niementowski reaction. Back to the roots, Tetrahedron Lett. 43 (2002) 3911–3913, https://doi.org/10.1016/S0040-4039(02)00619-6.

[33] S.K. Kundu, M.P.D. Mahindaratne, M.V. Quintero, A. Bao, G.R. Negretea, One-pot reductive cyclization to antitumor quinazoline precursors, Arkivoc 2008 (2008) 33–42, https://doi.org/10.3998/ark.5550190.0009.205.

[34] P. Kumar, D. Stypinski, H. Xia, A.J.B. Mcewan, H.J. Machulla, A simple and highly efficient process for synthesis of gefitinib and its intermediate, Indian J. Chem. B. 53B (2014) 1269–1274. http://nopr.niscair.res.in/handle/123456789/29472.

[35] B.S. Joshi, H.K. Desai, S.W. Pelletier, Synthesis of Pratorimine, J. Nat. Prod. 49 (1986) 445–448, https://doi.org/10.1021/np50045a010.

[36] C.J. Helal, Z. Kang, X. Hou, J. Pandit, T.A. Chappie, J.M. Humphrey, E.S. Marr, K. F. Fennell, L.K. Chenard, C. Fox, C.J. Schmidt, R.D. Williams, D.S. Chapin, J. Siuciak, L. Lebel, F. Menniti, J. Cianfrogna, K.R. Fonseca, F.R. Nelson, R. O'Connor, M. MacDougall, L. McDowell, S. Liras, Use of structure-based design to discover a potent, selective, in vivo active phosphodiesterase 10A inhibitor lead series for the treatment of schizophrenia, J. Med. Chem. 54 (2011) 4536–4547, https://doi.org/10.1021/jm2001508.

[37] H.K. Gibson, Quinazoline Derivatives. PCT Int. Appl. WO 199633980, European Patent Office, 31 October 1996.

[38] Z.-K. Wan, S. Wacharasindhu, E. Binnun, T. Mansour, An efficient direct amination of cyclic amides and cyclic ureas, Org. Lett. 8 (2006) 2425–2428, https://doi.org/10.1021/ol060815y.

[39] S. Bai, S. Li, J. Xu, X. Peng, K. Sai, W. Chu, Z. Tu, C. Zeng, R.H. Mach, Synthesis and structure-activity relationship studies of conformationally flexible tetrahydroisoquinolinyl triazole carboxamide and triazole substituted benzamide analogues as sigma2 receptor ligands, J. Med. Chem. 57 (2014) 4239–4251, https://doi.org/10.1021/jm5001453.

[40] D. Rodríguez-Hernandez, A.J. Demuner, L.C.A. Barbosa, L. Heller, R. CSUK. Novel hederagenin–triazolyl derivatives as potential anti-cancer agents, Eur. J. Med. Chem. 115 (2016) 257–267. http://dx.doi.10.1016/j.ejmech.2016.03.018.
[41] L.V. Lee, M.L. Mitchell, S.J. Huang, V.V. Fokin, K.B. Sharpless, C.-H. Wong, A potent and highly selective inhibitor of human alpha-1,3-fucosyltransferase via click chemistry, J. Am. Chem. Soc. 125 (2003) 9588–9589, https://doi.org/10.1021/ja0302836.
[42] S. Rohilla, S.S. Patel, N. Jain, Copper Acetate Catalyzed Regio-selective Synthesis of Substituted 1,2,3-Triazoles: A Versatile Azide–Alk-ene Cycloaddition/Oxidation Approach, Eur. J. Org. Chem. (2016) 847–854, https://doi.org/10.1002/ejoc.201501301.
[43] M.V.N. Souza, K.C. Pais, C.R. Kaiser, M.A. Peralta, M.L. Ferreira, M.C.S. Lourenço, Synthesis and in vitro antitubercular activity of a series of quinoline derivatives, Bioorg. Med. Chem. 17 (2009) 1474–1480, https://doi.org/10.1016/j.bmc.2009.01.013.
[44] S.F.P. Braga, L.C.M., E.B. da Silva, P.A. Sales Jr, S.M.F. Murta, A.J. Romanha, W.T. Soh, H. Brandstetter, R.S. Ferreira, R.B. de Oliveira. Synthesis and biological evaluation of potential inhibitors of the cysteine proteases cruzain and rhodesain designed by molecular simplification, Bioorg. Med. Chem. 25(6) (2017) 1889–1900. http://dx.doi.10.1016/j.bmc.2017.02.009.
[45] I.A. Moussa, S.D. Banister, C. Beinat, N. Giboureau, A.J. Reynolds, M. Kassiou, Design, Synthesis, and Structure−Affinity Relationships of Regioisomeric N-Benzyl Alkyl Ether Piperazine Derivatives as σ-1 Receptor Ligands, J. Med. Chem. 53 (2010) 6228–6239, https://doi.org/10.1021/jm100639f.
[46] S. Wertz, S. Kodama, A. Studer, Amination of benzoxazoles and 1,3,4-oxadiazoles using 2,2,6,6-tetramethylpiperidine-N-oxoammonium tetrafluoroborate as an organic oxidant, Angew. Chem. Int. Ed. 50 (2011) 11511–11515, https://doi.org/10.1002/anie.201104735.
[47] J.Z. Long, X. Jin, A. Adibekian, W. Li, B.F. Cravatt, Characterization of Tunable Piperidine and Piperazine Carbamates as Inhibitors of Endocannabinoid Hydrolases, J. Med. Chem. 53 (2010) 1830–1842, https://doi.org/10.1021/jm9016976.
[48] C. Zhang, C. Tan, X. Zu, X. Zhai, F. Liu, B. Chu, X. Mac, Y. Chen, P. Gong, Y. Jiang, Exploration of (S)-3-aminopyrrolidine as a potentially interesting scaffold for discovery of novel Abl and PI3K dual inhibitors, Eur. J. Med. Chem. 46 (2011) 1404–1414, https://doi.org/10.1016/j.ejmech.2011.01.020.
[49] X.S. Wang, H. Tang, A. Golbraikh, A. Tropsha, Combinatorial QSAR Modeling of Specificity and Subtype Selectivity of Ligands Binding to Serotonin Receptors 5HT1E and 5HT1F, J. Chem. Inf. Model. 48 (2008) 997–1013, https://doi.org/10.1021/ci700404c.
[50] P. Larsson, H. Engqvist, J. Biermann, E.W. Rönnerman, E. Forssell-Aronsson, A. Kovács, P. Karlsson, K. Helou, T.Z. Parris, Optimization of cell viability assays to improve replicability and reproducibility of cancer drug sensitivity screens, Sci. Rep. 10 (2020) 5798, https://doi.org/10.1038/s41598-020-62848-5.
[51] H.-Y. Chen, J. Villanueva, Playing Polo-Like Kinase in NRAS-Mutant Melanoma, J. Investig. Dermatol. 135 (2015) 2352–2355, https://doi.org/10.1038/jid.2015.253.
[52] E. Jasek-Gajda, H. Jurkowska, M. JasiŃska, J.A. Litwin, G.J. Lis, Combination of ERK2 and STAT3 Inhibitors Promotes Anticancer Effects on Acute Lymphoblastic Leukemia Cells, Cancer Genom. Proteomics 17 (2020) 517–527, https://doi.org/10.21873/cgp.20208.
[53] R. Roskoski Jr., Targeting ERK1/2 protein-serine/threonine kinases in human cancers, Pharmacol. Res. 142 (2019) 151–168, https://doi.org/10.1016/j.phrs.2019.01.039.
[54] T. Yamamoto, M. Ebisuya, F. Ashida, K. Okamoto, S. Yonehara, E. Nishida, Continuous ERK activation downregulates antiproliferative genes throughout G1 phase to allow cell-cycle progression, Curr. Biol. 16 (2006) 1171–1182, https://doi.org/10.1016/j.cub.2006.04.044.
[55] S. Meloche, J. Pouysségur, The ERK1/2 mitogen-activated protein kinase pathway as a master regulator of the G1- to S-phase transition, Oncogene 26 (2007) 3227–3239, https://doi.org/10.1038/sj.onc.1210414.
[56] J.-H. Ma, L. Qin, X. Li, Role of STAT3 signaling pathway in breast cancer, Cell Commun. Signal. 18 (2020), https://doi.org/10.1186/s12964-020-0527-z.
[57] J.M. Ku, S.R. Kim, S.H. Hong, H.-S. Choi, H.S. Seo, Y.C. Shin, S.-G. Ko, Cucurbitacin D induces cell cycle arrest and apoptosis by inhibiting STAT3 and NF-κB signaling in doxorubicin-resistant human breast carcinoma (MCF7/ADR) cells, Mol. Cell. Biochem. 409 (2015) 33–43, https://doi.org/10.1007/s11010-015-2509-9.
[58] J.-C. Chambard, R. Lefloch, J. Pouysségur, P. Lenormand, ERK implication in cell cycle regulation, Biochim. Biophys. Acta 1773 (2007) 1299–1310, https://doi.org/10.1016/j.bbamcr.2006.11.010.
[59] R. Hoshino, Y. Chatani, T. Yamori, T. Tsuruo, H. Oka, O. Yoshida, Y. Shimada, S. Ari-I, H. Wada, J. Fujimoto, M. Kohno, Constitutive activation of the 41-/43-kDa mitogen-activated protein kinase signaling pathway in human tumors, Oncogene 18 (1999) 813–822, https://doi.org/10.1038/sj.onc.1202367.
[60] V.B. Souza, D.F. Kawano, Structural basis for the design of allosteric inhibitors of the Aurora kinase A enzyme in the cancer chemotherapy, Biochim. Biophys. Acta Gen. Subj. 1864 (2020), https://doi.org/10.1016/j.bbagen.2019.129448.
[61] K. Stierand, M. Rarey, PoseView - molecular interaction patterns at a glance, J. Cheminform. 2 (2010) 50, https://doi.org/10.1186/1758-2946-2-S1-P50.
[62] E. Molden, B.H. Garcia, P. Braathen, A.E. Eggen, Co-prescription of cytochrome P450 2D6/3A4 inhibitor-substrate pairs in clinical practice. A retrospective analysis of data from Norwegian primary pharmacies, Eur. J. Clin. Pharmacol. 61 (2005) 119–125, https://doi.org/10.1007/s00228-004-0877-2.
[63] B. Yu, J. Duan, H. Ning, Y. Huang, B. Ling, F. Lin, Pharmacokinetics and metabolism of ulixertinib in rat by liquid chromatography combined with electrospray ionization tandem mass spectrometry, J. Sep. Sci. 43 (2020) 1275–1283, https://doi.org/10.1002/jssc.201901139.
[64] D.E. Bloch, Review of PHYSPROP Database (Version 1.0), J. Chem. Inf. Model. 35 (1995) 328–329, https://doi.org/10.1021/ci00024a602.
[65] W.A. Yeudall, R.Y. Crawford, J. Ensley, K. Robbins, MTS1/CDK4I is altered in cell lines derived from primary and metastatic oral squamous cell carcinoma, Carcinogenesis 15 (1994) 2683–2686, https://doi.org/10.1093/carcin/15.12.2683.
[66] R.N. Goto, L.M. Sobral, L.O. Sousa, C.B. Garcia, N.P. Lopes, J. Marín-Prida, et al., Anti-cancer activity of a new dihydropyridine derivative, VdiE-2N, in head and neck squamous cell carcinoma, Eur. J. Pharmacol. 819 (2018) 198–206, https://doi.org/10.1016/j.ejphar.2017.12.009.
[67] D.F. Kawano, M.R. Carvalho, M.F.M. Machado, A.K. Carmona, G.U.L. Braga, I. Carvalho, Biological and in silico studies on synthetic analogues of tyrosine betaine as inhibitors of neprilysin, a drug target for the treatment of heart failure, Curr. Pharm. Des. 24 (2018) 1887–1892, https://doi.org/10.2174/1381612824666180515114236.
[68] L. Kagami, G. Neves, R.P. Rodrigues, V.B. Silva, V. Eifler-Lima, D.F. Kawano, Identification of a novel putative inhibitor of the Plasmodium falciparum purine nucleoside phosphorylase: exploring the purine salvage pathway to design new antimalarial drugs, Mol. Divers. 21 (2017) 677–695, https://doi.org/10.1007/s11030-017-9745-8.
[69] J.J. Sutherland, R.K. Nandigam, J.A. Erickson, M. Vieth, Lessons in Molecular Recognition 2: Assessing and Improving Cross-Docking Accuracy, J. Chem. Inf. Model. 47 (2007) 2293–2302, https://doi.org/10.1021/ci700253h.
[70] R.A. Friesner, J.L. Banks, R.B. Murphy, T.A. Halgren, J.J. Klicic, D.T. Mainz, M. P. Repasky, E.H. Knoll, D.E. Shaw, M. Shelley, J.K. Perry, P. Francis, P.S. Shenkin, Glide: a new approach for rapid, accurate docking and scoring. 1. Method and assessment of docking accuracy, J. Med. Chem. 47 (2004) 1739–1749, https://doi.org/10.1021/jm0306430.